J. Phys. A: Math. Gen. **30** (1997) 2263–2280. Printed in the UK PII: S0305-4470(97)79371-5

The vortex dynamics analogue of the restricted three-body problem: advection in the field of three identical point vortices

Z Neufeld† and T Tél‡

† Department for Atomic Physics, Eötvös University, Puskin u. 5–7, H-1088 Budapest, Hungary
‡ Institute for Theoretical Physics, Eötvös University, Puskin u. 5–7, H-1088 Budapest, Hungary

Received 7 November 1996

Abstract. The passive advection of tracers in the field of three identical point vortices is considered as the hydrodynamical analogue of the restricted three-body problem. The chaotic motion is analysed by means of two-dimensional maps, its parameter dependence, Lyapunov exponents and topological entropies. The latter can be obtained as the growth rate of a dye droplet's perimeter in time. Similarities and differences of the vortex and gravitational problem are discussed.

1. Introduction

The dynamics of point vortices in an ideal two-dimensional incompressible fluid has attracted great recent attention [1–16] These vortices mutually interact: the centres undergo a passive advection, i.e. their velocity takes on the value of the velocity field generated by the others instantaneously. The recent interest in this subject is due to the fact that the motion of a low number of vortices can already be chaotic. It is known from the classical papers of Kirchhoff and other researchers [1, 17, 18] that the vortex dynamics can be described as a Hamiltonian system. For unbounded fluid otherwise at rest, the Hamiltonian of N vortices appears in the form

$$H(\{x_i, y_i\}) = -\frac{1}{\pi}\sum_{i<j}\kappa_i\kappa_j \ln r_{i,j} \tag{1}$$

where x_i and y_i are the coordinates of vortex i of strength κ_i, and $r_{i,j} = ((x_i - x_j)^2 + (y_i - y_j)^2)^{1/2}$ stands for the distance between vortices i and j. The dynamics is represented by the canonical equations:

$$\kappa_i \dot{x}_i = \frac{\partial H}{\partial y_i} \qquad \kappa_i \dot{y}_i = -\frac{\partial H}{\partial x_i} \qquad i = 1, 2, \ldots, N. \tag{2}$$

Since the Hamiltonian, H, does not depend on time explicitly, its value $E = H(\{x_i, y_i\})$ is a constant of the motion. In analogy with point mechanics, E can be called the energy of the vortex system. The invariance of H under translation and rotation implies the conservation laws [19]

$$\sum_i \kappa_i x_i = \text{constant} \qquad \sum_i \kappa_i y_i = \text{constant} \tag{3}$$

0305-4470/97/062263+18$19.50

and

$$\sum_i \kappa_i (x_i^2 + y_i^2) = \text{constant} \tag{4}$$

respectively. If the sum of all vortex strengths is nonzero, equation (3) defines a centre of vorticity that is fixed relative to the fluid, and can be used as a fixed point of reference. In view of equation (2), $p_i \equiv \kappa_i y_i$ can be considered as a canonical momentum. The deviation of equation (4) from the usual angular momentum is due to the fact that the invariance against rotation holds now in the (x, p) (coordinate-'momentum') plane. For $N > 3$ the dynamics is typically chaotic [4].

At this point it is worth recalling the celestial mechanical N-body problem [20, 21]. Restricting, for simplicity, the motion to the (x, y) plane, the Hamiltonian reads as

$$H(\{x_i, y_i, p_{x,i}, p_{y,i}\}) = \sum_i \frac{p_{x,i}^2 + p_{y,i}^2}{2m_i} - \gamma \sum_{i<j} \frac{m_i m_j}{r_{i,j}} \tag{5}$$

where x_i and y_i are the coordinates of the point mass m_i, and γ denotes the gravitational constant. The canonical equations are

$$\dot{x}_i = \frac{\partial H}{\partial p_{x,i}} \qquad \dot{p}_{x,i} = -\frac{\partial H}{\partial x_i} \qquad \dot{y}_i = \frac{\partial H}{\partial p_{y,i}} \qquad \dot{p}_{y,i} = -\frac{\partial H}{\partial y_i} \qquad i = 1, 2, \ldots, N. \tag{6}$$

The energy $E = H(\{x_i, y_i\})$ is again a constant of the motion. The invariance of H under translation and rotation in the (x, y) plane implies the conservation of momentum and angular momentum, respectively [22]. Due to the Galilean invariance of the equations of motion, there are two further integrals of motion, the two coordinates of the centre of mass. This problem is well known to be nonintegrable for $N > 2$ [20].

The difference in the number of vortices and point masses which mark the limit of integrability is related to the number of independent variables. By this we mean the number of variables governed by independent first-order differential equations, taking into account the global conservation laws. The difference is due to the different character of the velocity- and force-field mediating the interactions. The total number of first-order differential equations ($2N$ and $4N$), and the number of conserved quantities (4 and 6) provide us the number of independent variables: $2N$–4 and $4N$–6 in the N-vortex, and in the N-body problem, respectively. For general integrability this number must not be larger than two, which leads to the different limit numbers mentioned above.

A problem related to the vortex dynamics and of hydrodynamical relevance is the *advection* of passive tracer particles in the flow of the vortices [23–35]. The tracer is a test particle having no influence on the flow field, therefore, it can be considered as a special vortex of strength zero. Consequently, the advection in the field of N vortices is a problem of the same complexity as the $(N + 1)$-vortex dynamics [4].

The celestial mechanical analogue of passive advection is the motion of a small satellite whose mass is negligible compared with those of the celestial bodies and does not influence thus the gravitational field of the latter. The simplest two-dimensional problem of this type is the celebrated restricted three-body problem whose nonintegrability was shown by Poincaré [20]. The celestial bodies in this model are two point sources of equal mass rotating around their common centre of mass on circular orbits with a constant angular velocity.

The closest fluid dynamical analogue of this is the passive advection in the field of two vortices of equal strength which also rotate on circular orbits with a constant angular velocity. The motion in this case is regular [36] since the two-dimensional flow field is

stationary in the co-rotating frame. This also follows from the observation that the model is a special case of the three vortex problem and cannot be chaotic. The simplest *chaotic* vortex problem analogue of the restricted three-body problem is the advection by three vortices of equal strength. We shall see that the centres do not move then on circular orbits, but have nevertheless an average angular velocity. In a reference frame co-rotating with this angular velocity, the advection of a passive tracer has similarities, but also differences, to the motion of the satellite in the restricted three-body problem. Our aim is to study in detail the advection problem in the field of three identical vortices, and to compare it briefly with the restricted three-body problem.

The advection problem has been studied in different contexts [2, 3]. Here we also present a detailed investigation of the parameter dependence. The strength of chaoticity is measured by the average Lyapunov exponent, and by a somewhat less conventional, independent parameter, the topological entropy. The latter naturally arises as the growth rate of a dye droplet's perimeter in time. The droplet dynamics can also be followed in the restricted three-body problem, we find, however, that the method cannot be used to measure topological entropy. We explain an essential feature of the three-body dynamics; the possibility of a collision with the centres, as a consequence of the Hamiltonian's local behaviour.

The paper is organized as follows. In section 2, the motion of three identical vortices is briefly summarized in terms of a spherical phase space representation. In section 3, the advection dynamics, and its parameter dependence is studied in terms of a stroboscopic map, the droplet dynamics, the Lyapunov exponent and the topological entropy. Section 4 is devoted to a brief summary of the restricted three-body problem. We discuss the possibility of its characterization by means of a particle ensemble (a droplet). Finally, in section 5 we give a comparison of the two problems by pointing out important similarities and differences.

2. The motion of three identical vortices

The three vortex problem was studied in classical papers of Novikov [2] and Aref [3] for identical and different vortices, respectively. For the identical vortices that we consider, equations (2) can be put into a dimensionless form using the transformations:

$$(x, y) \to (lx, ly) \qquad t \to \frac{\pi l^2}{\kappa} t \qquad E \to \frac{\kappa^2}{\pi} E. \tag{7}$$

Here l is a characteristic length scale, which can be chosen in view of (4) as

$$l = [(r_{1,2}^2 + r_{1,3}^2 + r_{2,3}^2)/3]^{1/2} \tag{8}$$

representing an average distance between the vortices. After transformation (7) the only free parameter is the dimensionless energy, E, of the motion.

The dynamics of three identical vortices can be seen as a superposition of a relative motion and a rotation of the whole system around the centre of vorticity. The relative motion is periodic with a period T. The global rotational motion can be characterized by measuring the angular displacement, $\Delta\varphi_0$, around the centre of vorticity between two identical triangular configurations that are separated in time by T. The corresponding angular velocity is then obtained as $\omega_{\mathrm{rot}} = \Delta\varphi_0/T$. The frequency of the relative motion, $\omega_{\mathrm{rel}} \equiv 2\pi/T$, and the frequency of the rotation, ω_{rot}, depend on E and are generally incommensurate, implying a quasiperiodic dynamics. In figure 1 we show the energy dependence of these frequencies obtained by numerical integration of equations (2) for $N = 3$ in its nondimensional form (7), (8).

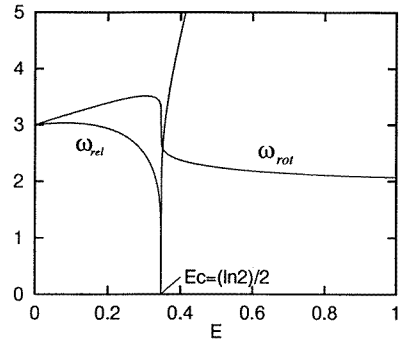

Figure 1. Energy dependence of the angular velocity corresponding to the rotating ($\omega_{\rm rot}$) and relative ($\omega_{\rm rel}$) motion of a system of three identical vortices. The right branch of $\omega_{\rm rel}(E)$ grows monotonically in the region not shown, i.e. for $\omega > 5$.

We briefly recall Novikov's results concerning different types of motion that can occur while changing the energy E. According to (7), (8) the product of all distances cannot be larger than unity, thus the dimensionless parameter E cannot be a negative number. For the following, it is convenient to also define the orientation of the vortex system σ, taking the value $+1$ and -1 when the vortices 1, 2 and 3 appear in anticlockwise and clockwise order, respectively.

For $E = 0$ the vortices form an equilateral triangle of unit edge size which rotates uniformly around the centre of vorticity without relative motion. At small positive energies, the vortices exhibit an oscillation around the equilateral configuration. In general, for $0 < E < E_{\rm c} \equiv (\ln 2)/2$ the triangle spanned by the vortices oscillates between two isosceles triangles, a sharp and a flat one (figures 2(a) and (b)). This oscillation in the shape of the triangle spanned by vortices is accompanied by the cyclic permutation of vortices (see also figures 4(a) and (d)). The system can never pass through a collinear configuration, so the orientation, σ, of the triangle remains unchanged in time.

The critical value $E = E_{\rm c}$ corresponds to a special kind of motion, a convergence to the collinear state of the vortices. This motion is aperiodic, as it is also indicated by the vanishing $\omega_{\rm rel}$ at this value of E.

For $E_{\rm c} < E < \infty$ the quantity σ is no longer conserved and a new characteristic of the trajectories is that two vortices remain closer to each other than to the third one during the motion (figures 2(c) and (d)). The triangle spanned by the vortices oscillates between two identical isosceles triangles having different signs of σ due to the exchange of the two near vortices by passing through the collinear state twice in one period (see also figures 4(e)–(h)). As $E \to \infty$ the two vortices tend to coalesce and the dynamics converge to the two vortex problem where one of the vortices has double strength.

In order to eliminate the rotation, it is worth introducing a reference frame rotating uniformly with $\omega_{\rm rot}$ around the centre of vorticity in which the motion of the vortices is periodic. This leads to a considerable simplification of the trajectories.

In figure 2 we show trajectories in the (x, y) plane viewed both from the standing and from the co-rotating reference frame. The two examples are taken from the two energy intervals $E < E_{\rm c}$ and $E > E_{\rm c}$ with qualitatively different dynamics.

Since the number of independent variables in the relative motion is two, the phase space is two-dimensional. In order to give a representation more reminiscent to point mechanics, we propose a different phase diagram than the one used by Novikov [2], and it can be seen

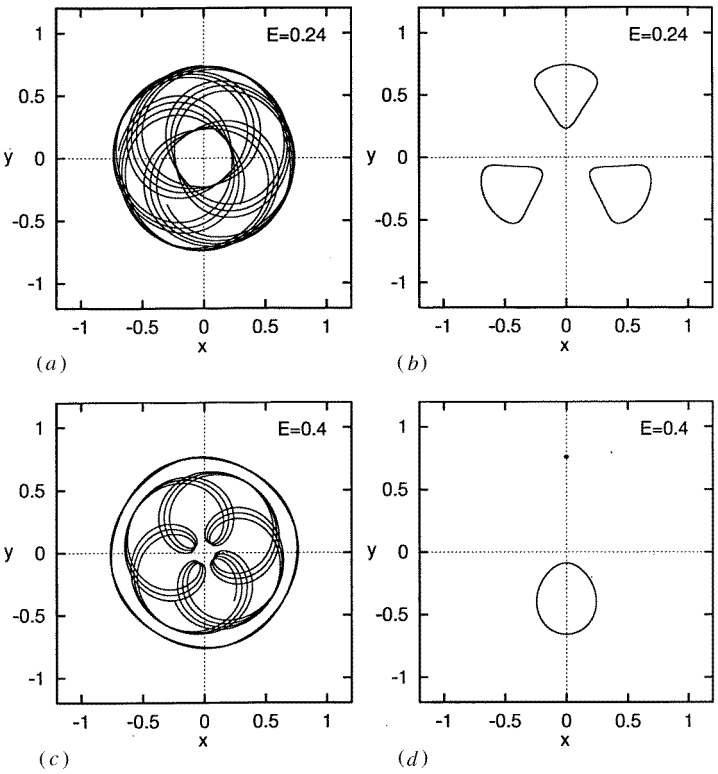

Figure 2. Trajectories of the three vortices viewed from the standing (*a*), (*c*) and from the co-rotating (*b*), (*d*) reference frame for $E = 0.24 < E_c \approx 0.346$ and $E = 0.4 > E_c$. The initial conditions are isosceles configurations symmetric to the vertical axis. Because of the invariance against exchange, the trajectories of the two lower vortices coincide in (*d*).

as a modified version of the representation introduced by Aref [3]. We define a phase space on the surface of the unit sphere (figure 3(*a*)) on which a point can be determined by means of two spherical angular coordinates related to the vortex system according to

$$\theta = \sigma \arcsin\frac{4A}{\sqrt{3}} = \sigma \arcsin\frac{\sqrt{3}(2r_{2,3}^2r_{1,3}^2 + 2r_{1,3}^2r_{1,2}^2 + 2r_{2,3}^2r_{1,2}^2 - r_{2,3}^4 - r_{1,3}^4 - r_{1,2}^4)^{1/2}}{r_{1,2}^2 + r_{1,3}^2 + r_{2,3}^2}$$
$$\varphi = \arccos\frac{\sqrt{3}(r_{1,3}^2 - r_{1,2}^2)}{2(r_{2,3}^4 + r_{1,3}^4 + r_{1,2}^4 - r_{2,3}^2r_{1,3}^2 - r_{1,3}^2r_{1,2}^2 - r_{2,3}^2r_{1,2}^2)^{1/2}} \tag{9}$$

where A denotes the area of the triangle spanned by the vortices. We note that φ can be obtained as an angle variable deducible from the planar phase diagram of [3]. Thus, a projection of our phase diagram to a horizontal plane gives something similar to that used by Aref. For a better visualization we also show a projection to a vertical cylindrical surface concentric with the sphere (figure 3(*b*)).

This phase space illustrates the symmetry properties of the relative dynamics: (i) the transformation $\sigma \leftrightarrow -\sigma$ corresponds to a reflection with respect to the equatorial plane, and (ii) the cyclic permutation of the vortices corresponds to a horizontal rotation $\varphi \leftrightarrow \varphi \pm 2\pi/3$.

The curves in figure 3 are labelled by different energy values. Now we can identify the fundamental points and curves corresponding to the motion of vortices. The elliptic fixed

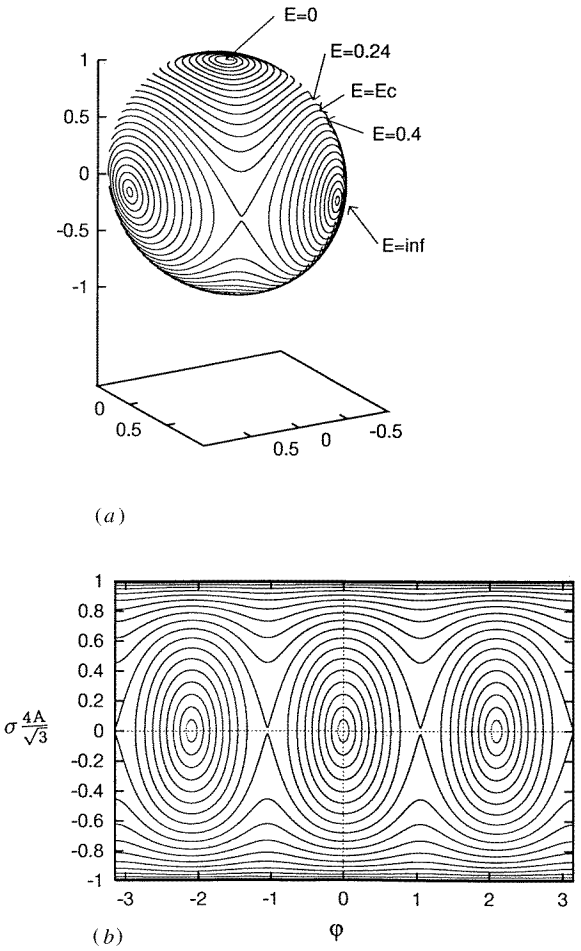

Figure 3. The phase space of the three vortex problem. (*a*) A spherical phase diagram defined in terms of the azimuthal angle, θ, and the rotational angle, φ, of equation (9). (*b*) The phase portrait projected on a vertical cylindrical surface concentric with the sphere which has a form characteristic for integrable Hamiltonian point mechanics.

points on the poles belong to the equilateral configuration at $E = 0$. The three other ones on the equator ($\theta = 0$) represent the case $E = \infty$ when two vortices coincide. The hyperbolic points on the equator belong to the symmetric collinear configuration of the vortices. The curve connecting them is labelled by the critical energy E_c, and is a separatrix lying on the boundary between regions in which the trajectory has different symmetry properties: invariance against the exchange of any pair of vortices, and against the cyclic permutation of all three vortices. The trajectories corresponding to figure 2 are also indicated by arrows in figure 3(*a*).

3. The advection problem

The advection of passive tracers is determined by the underlying velocity field. In the case of two-dimensional incompressible flows this can be expressed by using the streamfunction

$\psi(x, y, t)$ whose derivatives give the velocity components as

$$v_x(x, y, t) = \frac{\partial \psi}{\partial y} \qquad v_y(x, y, t) = -\frac{\partial \psi}{\partial x}. \tag{10}$$

The velocity field of a single point vortex consists of a circular vector field of modulus $\kappa\pi/r$, r being the distance from the centre. This is an irrotational flow everywhere except the centre. The streamfunction in this case is $-(\kappa/\pi)\ln r$. For a system of N vortices, the velocity fields are superimposed because of the linearity of the governing Laplace equation, and the streamfunction is:

$$\psi(x, y, t) = -\sum_i \frac{\kappa_i}{\pi} \ln r_i(t). \tag{11}$$

Due to the motion of vortices, ψ is time dependent through $r_i(t)$ which stands for the distance between the point (x, y) and vortex i at time t.

In the case of three identical vortices, the time dependence of ψ is two-frequency quasiperiodic. For the advection problem it is also convenient to introduce a reference frame co-rotating with the average angular velocity ω_{rot} of the whole system, as described in the previous section. In the co-rotating system the dimensionless streamfunction, measured in units of κ/π, can be written as

$$\tilde{\psi} = -\sum_i \ln r_i(t) - \frac{\omega_{\text{rot}}(x^2 + y^2)}{2}. \tag{12}$$

Note that the only parameter of $\tilde{\psi}$ is the vortex energy E. In figure 4 we show the time dependence of instantaneous streamlines for the two representative energy values of figure 2.

The dynamics of passively advected tracers is given in the co-rotating frame by:

$$\dot{x} = \frac{\partial \tilde{\psi}(x, y, t)}{\partial y} \qquad \dot{y} = -\frac{\partial \tilde{\psi}(x, y, t)}{\partial x}. \tag{13}$$

Thus, the advection problem corresponds to a *periodically forced Hamiltonian dynamical system*. Because of the time dependence of $\tilde{\psi}$, the number of effective degrees of freedom is 1.5, allowing in general for chaotic motion (figure 5).

For the special values $E = 0$ or $E = \infty$ the relative motion of the vortices freezes in and the time dependence of the streamfunction $\tilde{\psi}$ disappears, i.e. we have a stationary flow in the co-rotating system. Obviously the tracer dynamics is then nonchaotic, the particles just follow the streamlines (the $\tilde{\psi} =$ constant curves). Some of the streamlines correspond to the elliptic fixed points, or the separatrices connecting the hyperbolic fixed points of the advection dynamics. In figures 6(a) and (b) we show the streamlines for these special cases.

The case $E = E_c$ is also special due to the asymptotically decaying character of the forcing, i.e. the relative motion of vortices. For initial conditions on the separatrix of the vortex system, first a nonstationary flow field is present resulting in chaotic motion of the tracers, but as the relative motion of the vortex system decays, the particle trajectories converge towards regular trajectories. So, this is some kind of transient chaos [37], but a rather trivial one being a simple consequence of the transient character of forcing. If the vortex positions correspond to one of the hyperbolic fixed points, a similar situation is obtained (figure 6(c)) as in the previous special cases. The main difference is that in this case the state of the vortex system is unstable against perturbations.

Besides these special cases, we have a robust connected chaotic region among the vortices. In the hydrodynamical context, a strong mixing of the fluid takes place here, and therefore, we shall also call such extended chaotic regions, *mixing regions*. To visualize tracer dynamics we use a *stroboscopic* map on which we represent the position of the tracers

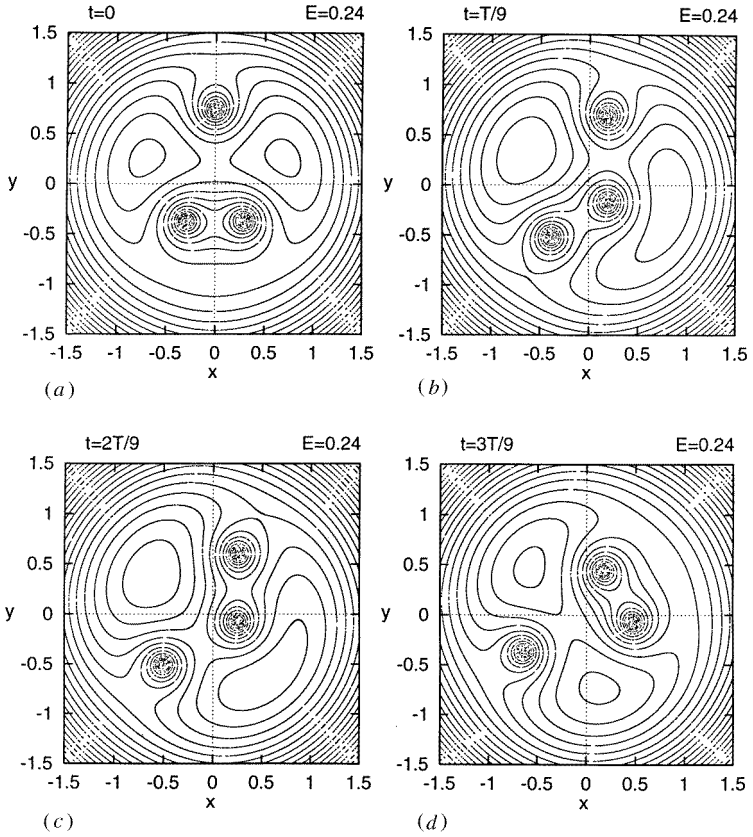

Figure 4. Instantaneous streamlines in the co-rotating frame for $E = 0.24$ at $t = 0$, $t = T/9$, $t = 2T/9$, $t = 3T/9$ (*a*)–(*d*); and $E = 0.4$ at $t = 0$, $t = T/6$, $t = 2T/6$, $t = 3T/6$ (*e*)–(*h*). Due to the permutation of the vortices, the relative motion is self-repeating for the rest of the period, with vortices permuted.

taking snapshots with a time difference T, where $T = 2\pi/\omega_{\rm rel}$ is the period of forcing, i.e. the period of the relative motion of vortices.

In figure 7 we show the stroboscopic maps for different representative energy values. As can be seen, the area occupied by the chaotic sea depends on E. When $E \ll E_{\rm c}$ or $E \gg E_{\rm c}$, this is restricted to the vicinity of the separatrices in the integrable cases shown in figures 6(*a*) and (*b*). As we depart from these cases in energy, the chaotic region is extending. We mention that, although the $E = E_{\rm c}$ case is asymptotically integrable, one does not necessarily observe an integrable behaviour on the stroboscopic map, due to the divergence of T. It is worth noting that the most extended chaotic sea seems to appear between $E = 0.25$ and 0.4. Even at these parameter values no chaos has been found very close to the vortex centres, in the vortex 'cores', and outside a circle with an approximate radius of 1.6. Despite the large extent of chaos, there appear to be elliptic islands outside of the cores in the chaotic sea. This becomes more pronounced when going below 0.25 or beyond 0.4 in the energy values. These islands are surrounded by usual KAM surfaces and contain chaotic bands inside.

The reason for having found no chaos in the vortex cores and in the outside region is due to the fact that the perturbation of the integrable Hamiltonian system is rather weak

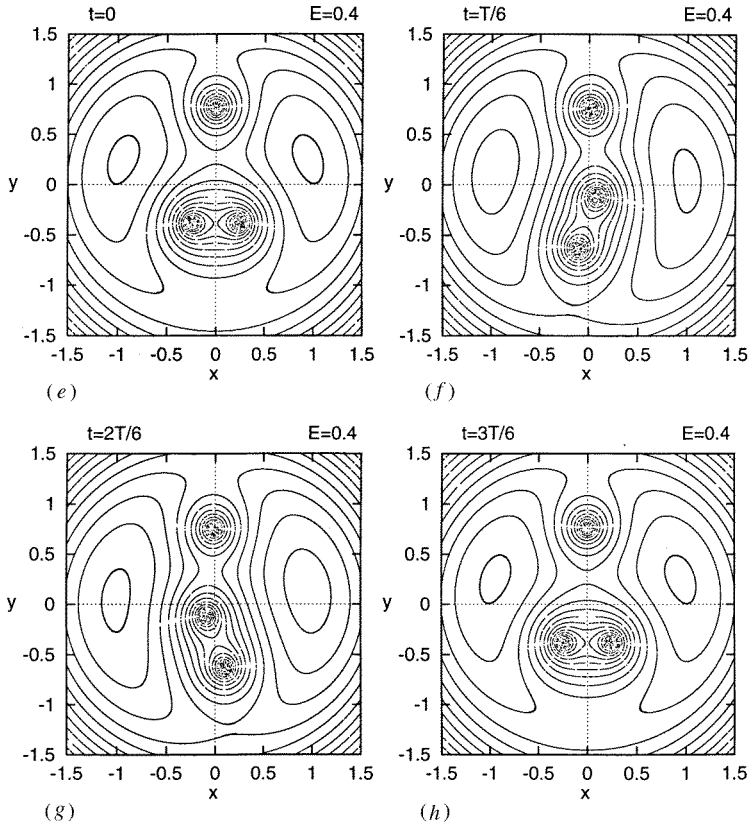

Figure 4. (Continued)

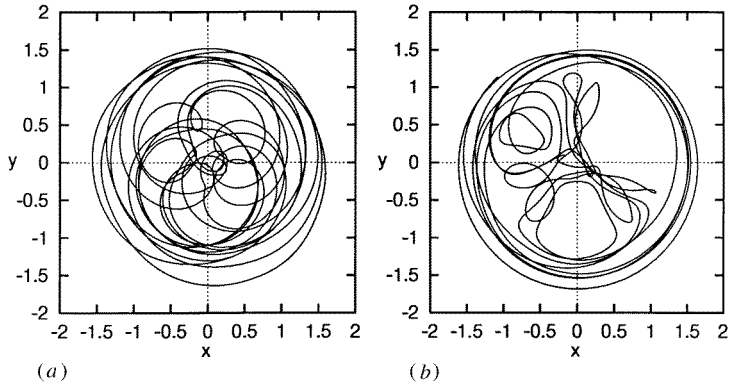

Figure 5. Chaotic tracer trajectory in the standing (*a*) and co-rotating (*b*) reference frame for $E = 0.24$. The initial condition for the tracer particle was $x = -0.175$ and $y = 0.1$.

in these regions. The effect of a given vortex close to its core is so pronounced that this leads to the suppression of chaos. We note that for $E > E_c$ three separate vortex cores can be observed, but when $E > E_c$, the two near vortices form a *common core* and thus, nonchaotic orbits connecting these two vortices also exist. The streamfunction, which plays

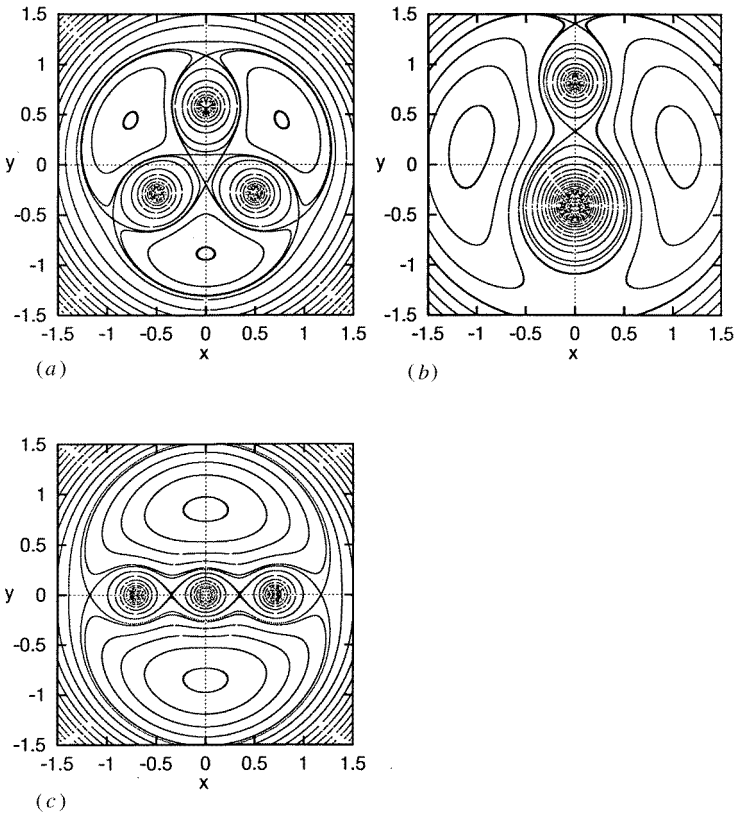

Figure 6. Streamlines in the co-rotating reference frame for special vortex configurations (*a*) $E = 0$, (*b*) $E = \infty$ and (*c*) $E = E_c$, hyperbolic fixed point. The flow in the co-rotating frame is stationary and streamlines coincide with tracer trajectories in these cases.

the role of the Hamiltonian, diverges as $\ln r$ when $r \to 0$. The perturbation due to the other vortices is basically constant in the vortex core. Thus, the relative weight of the perturbation is $1/\ln r$ and goes to zero when approaching the vortex centre.

Far from the vortex centres the velocity field is approximately the same as in the case of one single vortex of triple vortex strength. The corresponding streamfunction behaves like $\ln r$ when $r \to \infty$. The approximate strength of perturbation due to the relative motion of vortices can be obtained by expanding the streamfunction as $\ln(r+a) \approx \ln r + a/r$. Here a represents the finite relative displacement of the vortex centres during the motion. So the relative weight of the perturbing term is $1/r \ln r$ and decays to zero as $r \to \infty$.

These arguments explain the absence of chaos asymptotically close to the centres and infinitely far away from them. The mechanism that leads to the formation of vortex cores of *finite* sizes (and a finite circle around the three-vortex system outside of which the advection is nonchaotic) is still unclear and certainly deserves further attention.

In order to illustrate the difference in the mixing properties in the chaotic and nonchaotic regions, respectively, we show the evolution of a dye droplet injected into the flow at two different positions in figure 8. The numerical procedure used to follow the contour of the droplet has been carried out by adding interpolating particles whenever the distance between two adjacent particles becomes larger than a predefined small number. The droplet either

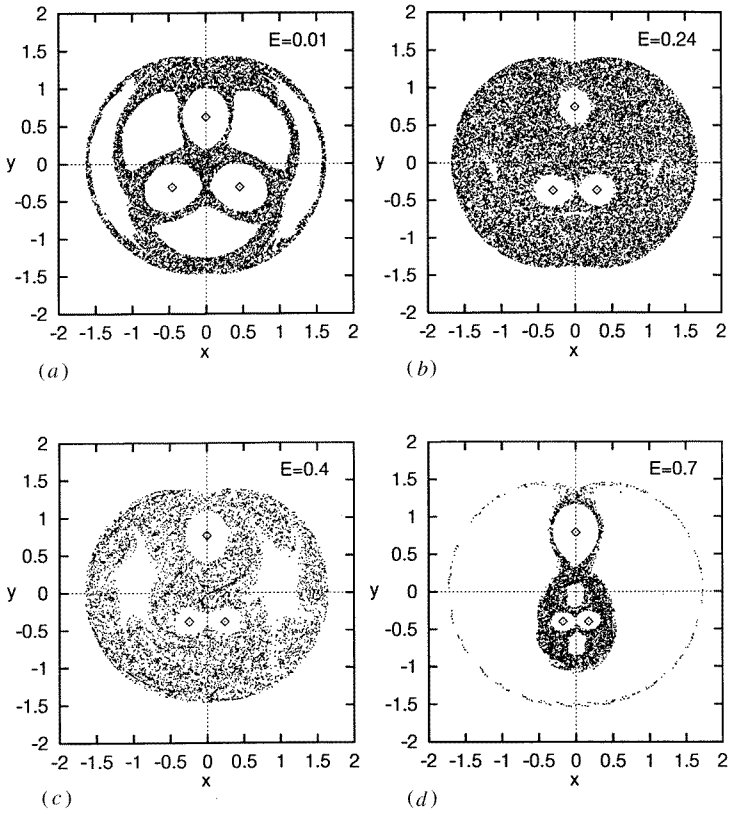

Figure 7. Stroboscopic maps obtained by trajectories started in the mixing region of the flow for (*a*) $E = 0.01$, (*b*) $E = 0.24$, (*c*) $E = 0.4$ and (*d*) $E = 0.7$. Dots represent intersections with the Poincaré plane for a single chaotic trajectory; initial conditions: (*a*)–(*c*) $(0.1, 0)$ and (*d*) $(0, 0.25)$.

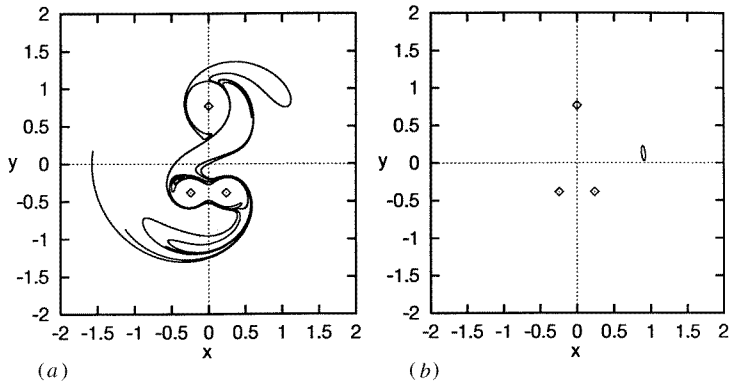

Figure 8. Contour of a dye droplet after a few periods, in the mixing (*a*), and nonmixing (*b*) region. The initially disk-shaped droplet of radius 0.05 was placed at $(0, 0)$ and $(1, 0)$, respectively. $E = 0.4$ in both cases. The contour was obtained by adding interpolating particles whenever the distances between two adjacent particles became larger than 0.005.

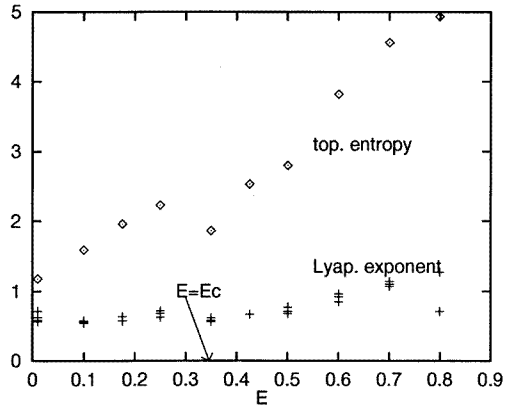

Figure 9. Energy dependence of the tracer dynamics' Lyapunov exponent and topological entropy.

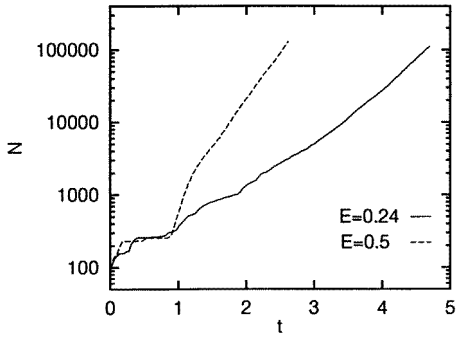

Figure 10. Time dependence of the number of particles (N) used to obtain the droplet contour by keeping the distance between adjacent particles smaller than 0.005. The initially disk-shaped droplet of radius 0.05 was placed at $(0.1, 0.1)$ for two energies, $E = 0.24$ and $E = 0.5$. The value of the topological entropy obtained from the slope of the $\ln N$ versus t curve is 2.23 and 2.80, respectively.

extends to the whole mixing region or it remains located in an island, depending on its initial condition.

For the quantitative characterization of the chaotic advection dynamics in the mixing region we calculated the Lyapunov exponents [38] for different energy values. The calculation was carried out by considering the length stretch of an infinitesimal segment ($dl = 10^{-4}$) averaged over a long-time trajectory ($t = 2000$). The results are summarized in figure 9. In the range $E < E_c$ the exponent is almost constant, falls down around E_c, and then increases again. This increase can be related to the steep increase of the mixing frequency, ω_{rel}, in this region. In the last region even if ω_{rel} increases further, the mixing region shrinks due to the convergence to an integrable case and the dynamics is dominated by the KAM tori forming the boundary of the mixing region. This results in a slow convergence of the Lyapunov exponent.

Another useful and independent characteristic of chaos can be extracted from the growth of the droplet contour's length. In the chaotic case an exponential growth can be observed, after some transient time, which depends on the initial size of the droplet (figure 10). The

corresponding exponent gives the characteristic number called *topological entropy* [38, 39] being a quantitative measure for the folding property of the chaotic dynamics. It has already been used to characterize the stretching of material lines in some hydrodynamical flows [28, 40, 41]. In figure 9 the value of the topological entropy is also presented for different energies; it has a similar trend as the Lyapunov exponent. Note that the topological entropy is always larger than the Lyapunov exponent in accordance with the fact that this entropy is an upper limit to the metric entropy [38] that coincides with the Lyapunov exponent in our case. From the continuous time Lyapunov exponents and topological entropies one can also obtain these quantities taken with respect to the stroboscopic map by simply multiplying their values by T.

4. The restricted three-body problem

As mentioned in the introduction, an analogy can be drawn between the advection problem described above and the restricted three-body problem of gravitationally interacting bodies. The restrictions consist of the following: (i) the mass of the third body is vanishingly small in comparison with the other ones ($m_3 \ll m_1, m_2$), so its effect on m_1 and m_2 is negligible; (ii) the two bodies of finite mass (m_1 and m_2) revolve in circles around their centre of mass; (iii) the light mass (m_3) moves in the orbital plane of the other two bodies. It follows from (i) that the motion of m_3 is determined by the other two bodies, but it exerts no force on them. So it can be considered as the 'advection' of m_3 by the rotating gravitational field of m_1 and m_2.

It is convenient to introduce a co-rotating reference frame in which m_1 and m_2 are fixed. In this system the dimensionless equations of motion for m_3 are [21]:

$$\dot{x} = v_x \qquad \dot{y} = v_y \qquad \dot{v}_x = 2v_y + \frac{\partial \Omega}{\partial x} \qquad \dot{v}_y = -2v_x + \frac{\partial \Omega}{\partial y} \tag{14}$$

where

$$\Omega = -\frac{1}{2}[(1-\mu)r_1^2 + \mu r_2^2] - \frac{1-\mu}{r_1} - \frac{\mu}{r_2} \tag{15}$$

is a kind of potentional energy, and

$$r_1 = \sqrt{(x-\mu)^2 + y^2} \qquad r_2 = \sqrt{(x+1-\mu)^2 + y^2} \tag{16}$$

is the distance from the two centres. The system has one dimensionless parameter, the reduced mass $\mu = m_2/(m_1 + m_2)$. Here we consider the case $m_1 = m_2$ ($\mu = 0.5$), in analogy with vortices of equal strengths.

The invariance against temporal translation in the co-rotating system results in a constant of motion,

$$E = \tfrac{1}{2}(\dot{x}^2 + \dot{y}^2) + \Omega \tag{17}$$

that is the dimensionless energy of m_3 in the co-rotating frame. ($C \equiv -2E$ is called the Jacobi integral [21].) Thus, the orbits in the four-dimensional phase space are lying in three-dimensional hypersurfaces defined by the condition $E =$ constant.

To have a simple representation of the possible orbits one can introduce a two-dimensional *Poincaré section* of such hypersurfaces [42]. A good representation can be obtained by the section $y = 0$ which means that whenever an orbit crosses the axis connecting the masses m_1 and m_2 from one side, we represent this event by a point in the (x, v_x) plane. We show such a Poincaré section in figure 11(a) for $E = -1.9$.

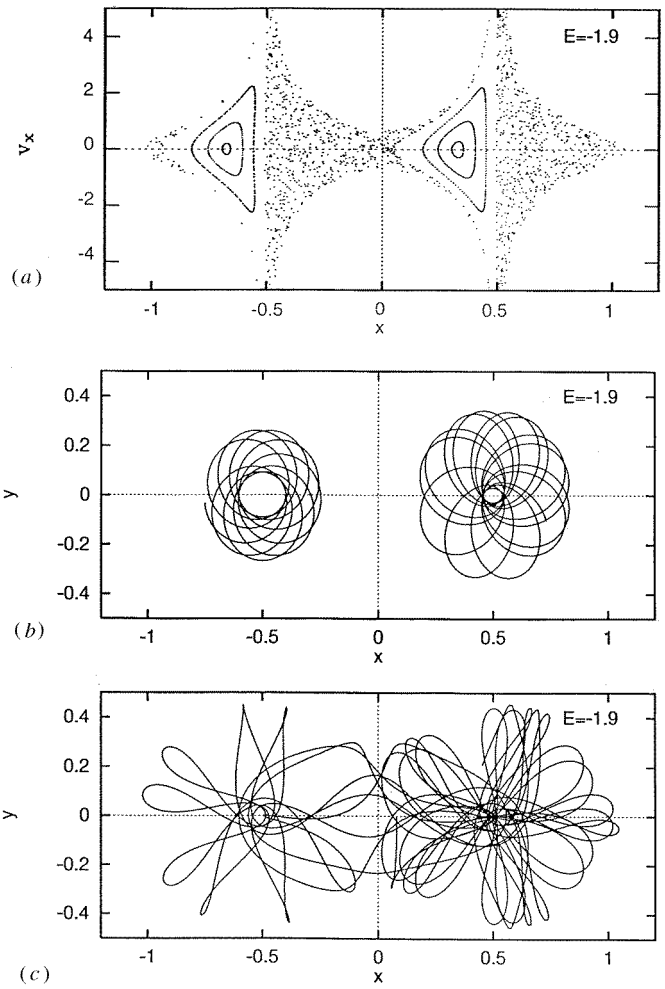

Figure 11. (*a*) Poincaré section of the restricted three-body problem for $E = -1.9$. The gravitational centres are placed at -0.5 and 0.5. Regular (*b*), and chaotic (*c*) orbits in the $x - y$ plane viewed from the co-rotating reference frame. Chaotic orbits can approach the gravitational centres arbitrarily close. Initial conditions: (*b*) $x = -0.4$, $y = 0$, $v_x = 0$, $v_y = 3.423\,45$ and $x = 0.6$, $y = 0$, $v_x = 0$, $v_y = 4.210\,39$; (*c*) $x = 0.1$, $y = 0$, $v_x = 0$, $v_y = 0.791\,619$.

Since the kinetic energy of m_3 cannot be negative, the trajectories must belong to the regions defined by the inequality $\Omega \leqslant E$. This results in an energy-dependent zero velocity boundary on the Poincaré plane. When $E < E_1 \approx -1.85$ this boundary intersects the x-axis. Thus, at the preselected value of $E = -1.9$, the phase space, which is accessible for the trajectories, splits into a bounded and unbounded component. The former is a finite compact region while the unbounded component extends to infinity.

In the bounded component there are orbits surrounding each of the two centres separately and others surrounding both of them. The former are mostly quasiperiodic (cf figure 11(*b*)) represented by closed curves on the Poincaré section and lie in a finite region on the left of the centres. The midpoints of these curve families corresponds to periodic trajectories bounded to one of the centres. The orbits surrounding both centres are typically chaotic but

this time chaotic orbits can come *arbitrarily close* to the centres (figure 11(*c*)). Thus, *no* gravitational 'cores' are created.

When changing the energy below E_1, the situation remains similar until reaching the value $E_2 \equiv -2.125$. When $E < E_2$ the bounded component of the phase space splits into two regions and the orbits surrounding both centres disappear. The behaviour around each centre remains, however, qualitatively unchanged, but the chaotic regions shrink and the regular orbits tend to dominate.

Finally, we note that in the unbounded component both regular and chaotic orbits are present. The latter ones correspond to a chaotic scattering [43, 44] of the small mass m_3. At $E = E_1$ the bounded and unbounded components merge, and in the energy range $E > E_1$ only a connected unbounded component exists.

For the quantitative characterization of the chaotic dynamics the corresponding Lyapunov exponent has been measured by different methods [42]. In analogy with the 'dye droplet experiment' one can also simulate the evolution of a continuously distributed ensemble of noninteracting particles in the gravitational field of m_1 and m_2. We have to follow the evolution of the ensemble on the Poincaré map.

Because the chaotic region contains singular points at $(\pm 0.5, 0)$, after some iterations the ensemble will have points arbitrarily close to these singularities and with arbitrarily large velocities, resulting in a contour with infinite length in finite time. This divergence is not a consequence of the chaotic dynamics and can be avoided by an appropriate transformation of the variables. This regularization is also required for the numerical integration. One possible method is the so-called global regularization of Birkhoff [21] based on the transformation

$$x = \frac{1}{4}\left(2\tilde{x} + \frac{\tilde{x}}{2(\tilde{x}^2+\tilde{y}^2)}\right) \qquad y = \frac{1}{4}\left(2\tilde{y} - \frac{\tilde{y}}{2(\tilde{x}^2+\tilde{y}^2)}\right)$$
$$\frac{\mathrm{d}t}{\mathrm{d}\tau} = \frac{(\tilde{x}^2-\tilde{y}^2-\frac{1}{4})^2 + 4\tilde{x}^2\tilde{y}^2}{4(\tilde{x}^2+\tilde{y}^2)^2} \tag{18}$$

where $\tilde{x}$, $\tilde{y}$ and τ are the new spatial and temporal variables, respectively.

As an example for a droplet shape, we show in figure 12 the contour of a small circle after six iterations on the Birkhoff regularized Poincaré map. The contour has evolved in a complicatedly winding curve similar to the advection problem.

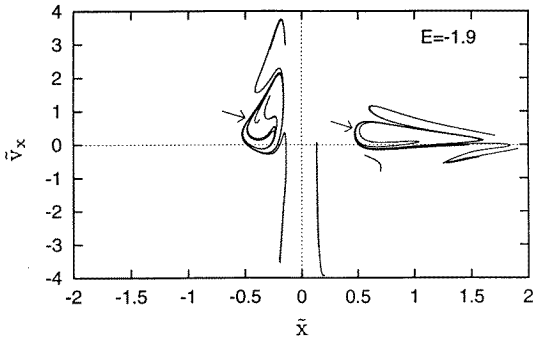

Figure 12. Contour of an ensemble after six iterations in the chaotic region of the Poincaré section defined by $\tilde{y} = 0$ in the regularized variables $\tilde{x}$ and $\tilde{v}_x$ ($\tilde{v}_x \equiv \mathrm{d}\tilde{x}/\mathrm{d}\tau$) at $E = -1.9$. The initially disk-shaped 'droplet' of radius 0.0004 was centred at $(\tilde{x} = -0.25, \tilde{v}_x = 0)$ on the Poincaré surface. Note that the initial connectedness of the ensemble is not preserved, in contrast to stroboscopic maps, due to orbits tangent to the Poincaré surface. The contour is coiled infinitely around two closed curves shown by arrows (see text).

It is natural to ask whether the topological entropy can be extracted from this procedure. Unfortunately, a further difficulty makes the determination of the topological entropy in this framework impossible. If the phase space contains such periodic orbits which do not intersect the Poincaré surface (and this cannot be avoided in general) then the ensemble might contain points which come arbitrarily close to these kind of orbits after some time. Thus, they can spend an arbitrarily long time around them and those who reach the Poincaré map again trace out pieces of the periodic orbits' unstable manifold [44]. Thus, at certain points the Poincaré map is ill defined and there can be an infinite number of such points. We conclude that due to this effect, namely the trapping by periodic orbits between two sections, Poincaré maps are not suitable to compute the topological entropy via the length of contour lines.

5. Discussion and conclusions

In this section we discuss the similarities and differences of the hydrodynamical advection problem and the restricted three-body problem.

As shown in section 3, the advection problem can be described by a Hamiltonian system of two nonautonomous differential equation, thus the number of effective degrees of freedom is 1.5. The gravitational problem is autonomous with 2 degrees of freedom, but due to the existence of the Jacobi constant, the number of effective degrees of freedom is reduced to 1.5 again. Thus, the trajectories are embedded in three-dimensional spaces in both cases, being problems with the minimal necessary complexity for chaotic behaviour. Furthermore, in both cases the structure of the phase space can be represented by two-dimensional sections, i.e. the dynamics can be described by means of two-dimensional maps.

A striking difference is that in the case of the restricted three-body problem, one has a continuum set of three-dimensional hypersurfaces with different values of the Jacobi constant. This energy parameter is *not* analogous to the energy of the vortex system. The latter one is just a tunable parameter characterizing the forcing, while the advected particles have no conserved energy-like quantity. The energy of the advection problem instead corresponds to the mass ratio, μ, of the three-body problem.

In both cases a co-rotating system of reference can be introduced. While in the gravitational problem this transformation makes the time dependence of the driving disappear, the quasiperiodic motion of vortices is reduced to a periodic time dependence. This allows for the introduction of a special kind of map, the stroboscopic map, in the advection problem.

In both cases of the structure of the phase space, there exists a chaotic 'mixing' region, some 'central' regions dominated by singularities and an 'asymptotic' region far from the singularities. In the two latter regions the trajectories are locally regular. The essential difference is that, while the advected particles, depending on their initial coordinates, remain in one of these regions forever, the small mass can enter and leave any of these three regions. This difference can be simply explained by the fact that for the advection problem in the field of a single vortex, which is relevant in the core and in the asymptotic region, the trajectories are concentric circles, but for the corresponding restricted two-body problem a continuous set of orbits is possible, ranging from circles to very elongated ellipses or even hyperbolas. The orbits with large eccentricities are responsible for the possibility of switching between different regions. Of course, also in the case of the restricted three-body problem there are orbits which stay in one of the three regions forever.

This is again a result of the difference between velocity- and force-fields that is in the dimensionality of the phase space (4 and 2) in these integrable elementary problems.

Thus, the local dynamics around the centres is characterized by trajectories lying on two-dimensional tori (defined by the conserved quantities) and circles, respectively, centred at the singular point. While the toroidal surfaces connect points close to the centre with ones further away, where the local approximation is no longer valid, this is not true in the case of concentric circles.

The fact that the particles advected by the flow in the mixing region will never get close to one of the point vortices makes the numerical integration of this problem much easier than that of the gravitational problem, where a regularization procedure is required, as mentioned in the preceding section.

Note that the argument above is independent of the number of singular points and their dynamics. The fact that gravitational centres lie in the chaotic region even in more complicated cases might be a reason for the relatively emptiness of the interplanetary region of the solar system. On the other hand, regular islands around the vortices seem to be a universal feature of advection in point vortex systems since they are also present in cases when the vortex centres move chaotically [14].

Finally, we note that the analogy between the restricted three-body problem and hydrodynamical advection has long been discussed in literature [20]. It was pointed out by Mulholland [45] that a realistic flow in which the advection fully corresponds to the equations of the restricted three-body problem cannot be found. Thus, the advection in the field of point vortices can only be a partial analogy. This is also expressed by the fact that the restricted two-vortex problem is integrable. On the other hand, the advection in the field of the three vortices is also an analogy of the restricted four-body problem [46] where the gravitational centres lie on the corners of an equilateral triangle. They rotate with a constant angular velocity, therefore the dynamics of the light mass is of a similar type as in the three-body case, just the geometry is different.

A more realistic celestial mechanical arrangement is the elliptic three-body problem when the two gravitational centres move along Kepler ellipses instead of circles. In this case however, the force acting on the third mass is time dependent even in the co-rotating frame, and no Jacobi integral exists. This dynamics of the light mass has thus a higher degree of freedom (2.5) than in the circular problem. In conclusion, we believe that the advection field of three point vortices is a very natural analogue of the classical restricted three-body problem, but the analogy is necessarily incomplete.

Acknowledgments

We thank B Érdi, Gy Károlyi, Z Kovács, H Lustfeld, A Provenzale, K G Szabó and T Vicsek for useful discussions. This work was partially supported by the Hungarian Science Foundation under grant nos OTKA T17493, T19483, T4439, T019299, and the US–Hungarian Science and Technology Joint Fund under project JFNo 501.

References

[1] Saffman P G 1992 *Vortex Dynamics* (Cambridge: Cambridge University Press)
[2] Novikov E A 1975 *Sov. Phys.–JETP* **41** 937
[3] Aref H 1979 *Phys. Fluids* **22** 393
[4] Aref H and Pomphrey N 1980 *Phys. Lett.* **78A** 297
[5] Aref H and Pomphrey N 1982 *Proc. R. Soc.* A **380** 359
[6] Aref H 1983 *Ann. Rev. Fluid Mech.* **15** 1
[7] Eckhardt B and Aref H 1988 *Phil. Trans. R. Soc.* A **326** 655
Eckhardt B 1988 *Europhys. Lett.* **5** 107

[8] Aref H, Jones S W, Mofina S and Zawadski I 1989 *Physica* **37D** 423
[9] Meleshko V V, Konstantinov M Yu, Gurzhi A A and Konovaljuk 1992 *Phys. Fluids* A **4** 2779
[10] Zanetti L and Franzese P 1994 *Physica* **76D** 99
[11] Meleshko V V 1994 *Phys. Fluids* **6** 6
[12] Rom-Kedar V, Leonard A and Wiggins S 1990 *J. Fluid Mech.* **214** 347
[13] Elhmaidi D, Provenzale A and Babiano A 1993 *J. Fluid Mech.* **257** 533
Provenzale A, Babiano A and Villone B 1995 *Chaos Solitons and Fractals* **5** 2055
[14] Babiano A, Boffetta G, Provenzale A and Vulpiani A 1994 *Phys. Fluids* **6** 2465
[15] Péntek Á, Tél T and Toroczkai Z 1995 *J. Phys. A: Math. Gen.* **28** 2191
Péntek Á, Tél T and Toroczkai Z 1995 *Fractals* **3** 33
[16] Boffetta G, Celani A and Franzese P 1996 *J. Phys. A: Math. Gen.* **29** 3749
[17] Lamb H 1932 *Hydrodynamics* (Cambridge: Cambridge University Press)
[18] Kochin N E, Kibel I A and Rose N V 1964 *Theoretical Hydrodynamics* (New York: Interscience)
[19] Chapman D M F 1978 *J. Math. Phys.* **19** 1988
[20] Poincaré H 1892 *Les Méthodes Nouvelles de la Mécanique Céleste* (New York: Dover)
Birkhofff G D 1912 *Rend. Circ. Mat. Palermo* **39** 1
Wintner A 1941 *The Analytical Foundations of Celestial Mechanics* (Princeton, NJ: Princeton University Press)
Murison M A 1989 *Astron. J.* **98** 2346
[21] Szebehely V 1967 *Theory of Orbits* (New York: Academic)
[22] Landau L D and Lifschitz I M 1960 *Classical Mechanics* (London: Pergamon)
[23] Aref H 1984 *J. Fluid Mech.* **143** 1
Khakhar D V, Rising H and Ottino J M 1987 *J. Fluid Mech.* **172** 419
[24] Aref H 1985 *Theoretical and Applied Mechanics* ed F I Niordson and N Olhoff (Amsterdam: North-Holland)
[25] Aref H and Balachandar S 1986 *Phys. Fluids* **29** 3515
[26] Chaiken J, Chevray R, Tabor M and Tan Q M 1986 *Proc. R. Soc.* A **408** 165
[27] Ottino J M 1989 *The Kinematics of Mixing: Stretching, Chaos and Transport* (Cambridge: Cambridge University Press)
Ottino J M 1990 *Ann. Rev. Fluid Mech.* **22** 207
Jana S C, Metcalfe G and Ottino J M 1994 *J. Fluid Mech.* **269** 199
[28] Crisanti A *et al* 1991 *Riv. Nuovo Cimento* **14** 1
[29] Muzzio F J, Swanson P D and Ottino J M 1992 *Int. J. Bifurc. Chaos* **2** 37
[30] Wiggins S 1992 *Chaotic Transport in Dynamical Systems* (Berlin: Springer)
[31] Solomon T H and Gollub J P 1988 *Phys. Rev.* A **38** 6280
Solomon T H, Weeks E R and Swinney H L 1994 *Physica* **76D** 70
[32] Sommerer J C and Ott E 1993 *Science* **259** 281
Sommerer J C 1994 *Physica* **76D** 85
[33] Pierrehumbert R T 1994 *Chaos Solitons and Fractals* **4** 1091
[34] Beigie D, Leonard A and Wiggins S 1994 *Chaos Solitons and Fractals* **4** 749
[35] Péntek Á, Toroczkai Z, Tél T, Grebogi C and Yorke J A 1995 *Phys. Rev.* E **51** 4076
[36] Newton P K 1994 *Physica* **79D** 416
[37] Tél T 1990 *Directions in Chaos* vol 3, ed Hao Bai-Lin (Singapore: World Scientific)
[38] Beck C and Schlögl F 1993 *Thermodynamics of Chaotic Systems* (Cambridge: Cambridge University Press)
Ott E 1993 *Chaos in Dynamical Systems* (Cambridge: Cambridge University Press)
[39] Newhouse S and Pignataro T 1993 *J. Stat. Phys.* **72** 1331
[40] Ziemniak E, Jung C and Tél T 1994 *Physica* **76D** 123
[41] Jung C and Ziemniak E 1994 *Fractals in the Natural and Applied Sciences* ed M M Novak (Amsterdam: North-Holland)
[42] Smith R H and Szebehely V 1993 *Celest. Mech. Dynam. Astron.* **56** 409
[43] Smilansky U 1992 *Chaos and Quantum Physics* ed M J Giannoni *et al* (New York: Elsevier)
Jung C 1992 *Acta Phys. Pol.* **23** 323
Ott E and Tél T 1993 *Chaos* **3** 417
[44] Kovács Z and Wiesenfeld L 1995 *Phys. Rev.* E **51** 5476
[45] Mulholland J D 1970 *Celest. Mech.* **1** 320
[46] Simó C 1978 *Celest. Mech.* **18** 165
Majorana A 1981 *Celest. Mech.* **25** 267
Casasayas J, Llibre J and Nunes A 1994 *Celest. Mech.* **60** 273.